Sparsity-Based High-Resolution Analysis of Mixed-Mode Over-The-Horizon Radar Signals

*Ammar Ahmad [1], Yimin D. Zhang [1 *], Braham Himed [2]*

[1] *Department of Electrical and Computer Engineering, Temple University, Philadelphia, PA 19122, USA*
[2] *Distributed RF Sensing Branch, Air Force Research Laboratory, WPAFB, OH 45433, USA*
**E-mail: ydzhang@temple.edu*

Keywords: Frequency estimation, fractional Fourier transform, group sparsity, over-the-horizon radar, ordinary and extraordinary modes

Abstract

Doppler frequency analysis is important in over-the-horizon radar (OTHR) in order to determine important target parameters such as the target altitude. In this paper, we analyze the Doppler signatures of OTHR signals propagated through both ordinary and extraordinary electromagnetic modes. As the signals following the two propagation modes undergo different group delays, the Doppler frequencies of a target associated with these two modes differ from each other. The frequency analysis of the resulting Doppler signatures becomes challenging when the Doppler components associated with these two modes are closely separated or even partially overlapping. In this paper, we develop a low-complexity sparsity-based method to resolve the Doppler signatures corresponding to the two propagation modes. It is based on a Lasso-based approach and the computational complexity is effectively reduced by employing a frequency focusing transform. To demonstrated the effectiveness of the proposed approach, simulation results are presented for challenging scenarios where the multipath Doppler signatures corresponding to the two propagation modes are interlaced or very close to each other.

1 Introduction

Sky-wave over-the-horizon radar (OTHR) systems provide effective early-warning surveillance capability as they enable localization and tracking of targets that are far beyond the earth horizon [1–5]. These objectives are achieved by transmitting a high-frequency (HF) band signal which reaches long-range targets after getting reflected from the ionosphere. OTHR target tracking, parameter estimation, and the suppression of interference and clutter motivated significant efforts in signal processing [6–11].

The operational frequencies of an OTHR depend on the ionospheric conditions. In practice, only a narrow signal bandwidth can be used, making accurate target parameter estimation, especially target altitude estimation, very challenging. Moreover, time-varying ionosphereic conditions add further uncertainties and make target altitude estimation more challenging. Existing target altitude estimation approaches can be broadly classified into three main categories: (a) tracking of target positions, including target altitude [7, 8, 10, 12–14]; (b) joint estimation of target and ionosphere parameters by exploiting their statistical models [11, 15]; and (c) time-frequency signal analysis of the Doppler signatures corresponding to the local multipath signals [16–26]. The proposed work considered in this paper is based on the last approach.

Due to the earth's magnetic field, the ionosphere is birefringent at radio frequencies. This results in two canonical propagation modes corresponding to the polarization of the radio waves, respectively regarded as the ordinary (O) and extraordinary (X) modes [27–29]. Measurements from vertical and oblique ionospheric sounders, which track the state of ionosphere, reveal that the signals propagating through the two polarization modes exhibit different group delays. It implies that the signals from the two modes are reflected from different vertical heights of the ionosphere. Due to different group delays or virtual ionosphere heights for the O- and X-mode signals, their corresponding Doppler signatures and slant ranges also differ. Existing methods developed for single-mode propagation, therefore, fail to work when the separation between the Doppler frequencies of the O/X-mode signals is closely separated.

In [30], the separation of O/X-mode signals with close or interlaced Doppler signatures was considered using the fractional Fourier transform. The target is assumed to move at a constant altitude with a constant horizontal velocity. By further extending this approach in the context of sparsity-based reconstruction, it was shown in [31] that Lasso [32] and group Lasso-based [33] strategies can be employed to provide high-resolution estimates of the mixed O/X-mode Doppler frequencies as well as their separation in the spectral domain. However, due to the large size of the search space of frequencies and the subsequent dictionary matrices employed in Lasso, the resulting algorithm requires high computational complexity. In this paper, we address this issue by employing a frequency focusing transform which enables computationally efficient Doppler frequency estimation. Compared to the existing techniques, the proposed strategy not only reduces the search space of the frequency estimation but also reduces the size of the data matrix

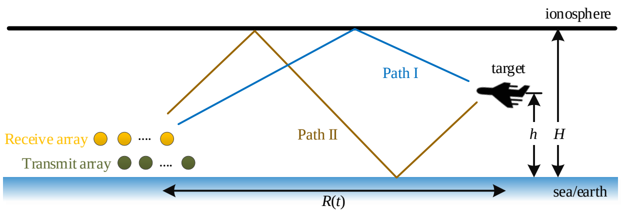

Fig. 1. Flat-earth local multipath propagation model of OTHR.

to be processed by the sparsity-based technique. Simulation results confirm the effectiveness of the proposed strategy.

Notations: Lower-case (upper-case) bold characters are used to denote vectors (matrices). $(.)^{\mathrm{T}}$ denotes the transpose operator of a matrix or vector. Moreover, $||\cdot||_1$ and $||\cdot||_2$ respectively denote the l_1- and l_2-norms of a vector.

2 Doppler Signature Analysis

A simplified flat-earth model of OTHR is illustrated in Fig. 1 where H denotes the ionosphere height, h is the target altitude, and $R(t)$ is the time-varying ground range of the target with respect to OTHR. As shown in the figure, a portion of the transmit signal is reflected by the target and travels back towards the radar to enable target detection, localization, and tracking. In addition to the direct path reflected only by the ionosphere layer (path I), the signals may also be reflected by the earth surface, yielding a local multipath propagation component (path II) [7]. This results in the following three distinct round-trip propagation paths: (a) transmitted and received along path I; (b) transmitted and received along path II; and (c) transmitted along path I and received along path II, and vice versa. The slant range equations for OTHR can be readily developed using the equivalent local multipath model shown in Fig. 2 where the propagation paths above the ionosphere are the mirrored versions of the ones below the ionosphere layer.

The OTHR signals following the O and X propagation modes undergo different group delays, effectively yielding reflections from different virtual heights in the ionosphere.

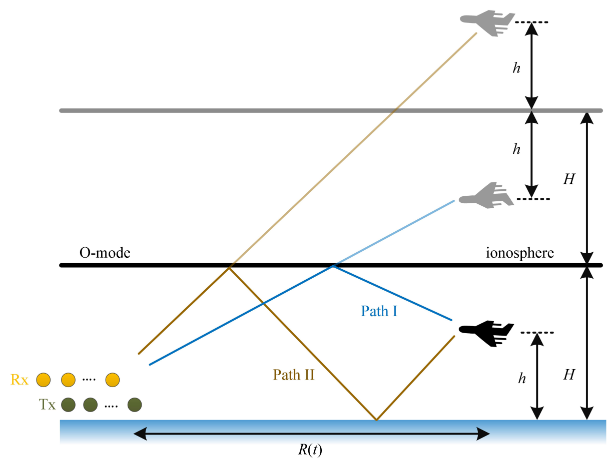

Fig. 2 Equivalent local multipath propagation model for the O-mode wave.

These virtual heights usually differ from each other depending on the operating frequency of the OTHR and the incidence angle of the transmitted signals [27–29]. Without loss of generality, we assume that the virtual ionosphere height of the X-mode wave is lower than that of the O-mode wave. In this context, we modify the single-layer multipath signal model into a two-layer model as shown in Fig. 3. Here, H denotes the virtual ionosphere height of the O-mode wave whereas $H-\Delta H$ represents that of the X-mode wave with $\Delta H \ll H$. The signals following each of the two propagation modes will have their corresponding three distinct multipath Doppler components because of the three round-trip paths available for each mode. Denote the Doppler frequencies of the received O- and X-mode signals as $f_{\mathrm{o},i}$ and $f_{\mathrm{x},i}$, respectively, where $i=1,2,3$ denotes the path index. Following [19, 30, 31], the Doppler frequencies of the two-mode signals can be expressed as:

$$\begin{aligned} f_{\mathrm{o},1} &= \bar{f}_{\mathrm{o}}+\Delta f_{\mathrm{o}}, \quad f_{\mathrm{o},2}=\bar{f}_{\mathrm{o}}-\Delta f_{\mathrm{o}}, \quad f_{\mathrm{o},3}=\bar{f}_{\mathrm{o}}, \\ f_{\mathrm{x},1} &= \bar{f}_{\mathrm{x}}+\Delta f_{\mathrm{x}}, \quad f_{\mathrm{x},2}=\bar{f}_{\mathrm{x}}-\Delta f_{\mathrm{x}}, \quad f_{\mathrm{x},3}=\bar{f}_{\mathrm{x}}, \end{aligned} \tag{1}$$

where $\bar{f}_{\mathrm{o}}$ and $\bar{f}_{\mathrm{x}}$ respectively denote the average Doppler component for O- and X-mode signals. Moreover, Δf_{o} and Δf_{x} correspond to the intra-mode difference Doppler components for signals following the O- and X-mode propagation, respectively. Note that the three Doppler components of each mode are equidistant and symmetric in the spectral domain [30, 31].

From [19, 30, 31], we know that

$$\bar{f}_{\mathrm{o}} \approx -\frac{2f_c}{c}\dot{R}+\frac{4f_cH^2\dot{R}}{cR^2}, \quad \Delta f_{\mathrm{o}} \approx -\frac{4f_cHh\dot{R}}{cR^2}, \tag{2}$$

where f_c is the carrier frequency, R is the target ground range, $\dot{R}=\mathrm{d}R/\mathrm{d}t$ denotes the target velocity, and c is the speed of electromagnetic waves. It is clear that all the Doppler frequencies are proportional to $\dot{R}$.

Since the only difference between the O- and X-mode signals is the virtual ionosphere heights, we can formulate the Doppler components corresponding to the X-mode by substituting H by $H-\Delta H$ in Eq. (2), given by

$$\begin{aligned} \bar{f}_{\mathrm{x}} &\approx -\frac{2f_c}{c}\dot{R}+\frac{4f_c(H-\Delta H)^2\dot{R}}{cR^2} \\ &= \bar{f}_{\mathrm{o}}-\frac{4f_c\dot{R}}{cR^2}(2H\Delta H-\Delta H^2), \\ \Delta f_{\mathrm{x}} &\approx -\frac{4f_c(H-\Delta H)h\dot{R}}{cR^2}=\Delta f_{\mathrm{o}}+4\frac{f_ch\dot{R}}{cR^2}\Delta H. \end{aligned} \tag{3}$$

The resulting noise-free form of the overall mixed O/X-mode signal $y(t)$ at the OTHR receiver is expressed as

$$y(t)=\sum_{i=1}^{3}\left(A_{\mathrm{o},i}e^{j(2\pi\int_0^t f_{\mathrm{o},i}\mathrm{d}t+\phi_{\mathrm{o},i})}+A_{\mathrm{x},i}e^{j(2\pi\int_0^t f_{\mathrm{x},i}\mathrm{d}t+\phi_{\mathrm{x},i})}\right), \tag{4}$$

for $0\le t\le T$, where $A_{\mathrm{o},i}$ and $A_{\mathrm{x},i}$ respectively denote the signal magnitudes for the signals following the O- and X-modes, $\phi_{\mathrm{o},i}$ and $\phi_{\mathrm{x},i}$ are the corresponding initial phases of the two modes, and T is the coherent processing interval (CPI). Note that $f_{\mathrm{o},i}$ and $f_{\mathrm{x},i}$ are time-varying.

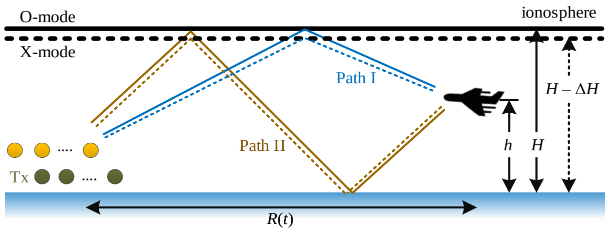

Fig. 3 Flat-earth local multipath propagation model of OTHR for mixed O/X-mode propagation.

Considering a typical scenario with $h \ll R$ and $\Delta H \ll R$, we observe the following relationship:

$$\bar{f}_{\mathrm{x}} \approx \bar{f}_{\mathrm{o}} - f_\delta, \quad \Delta f_{\mathrm{x}} \approx \Delta f_{\mathrm{o}}, \tag{5}$$

where $f_\delta \approx (4f_c\dot{R}/(cR^2))(2H\Delta H - \Delta H^2)$ is an unknown inter-mode Doppler difference illustrating the spectral separation between the average Doppler components of the signals associated with the two propagation modes.

From Eqs. (1)–(5), we observe that the inter-mode Doppler difference f_δ is shared by all the local multipath pairs of the corresponding O/X-mode signals, i.e.,

$$f_\delta = f_{\mathrm{o},i} - f_{\mathrm{x},i}, \quad i = 1, 2, 3. \tag{6}$$

This implies that the corresponding Doppler components of the O- and X-mode signals are displaced in the spectral domain by a common shift f_δ. Therefore, Eq. (4) can be rewritten in the following form:

$$\begin{aligned} y(t) = \sum_{i=1}^{3} \Big(& A_{\mathrm{o},i} e^{j(2\pi \int_0^t f_{\mathrm{o},i} \mathrm{d}t + \phi_{\mathrm{o},i})} \\ & + A_{\mathrm{x},i} e^{j(2\pi \int_0^t (f_{\mathrm{o},i}+f_\delta) \mathrm{d}t + \phi_{\mathrm{x},i})} \Big). \end{aligned} \tag{7}$$

If the inter-mode Doppler difference f_δ is large ($f_\delta \gg 3\Delta f_{\mathrm{o}}$), the resulting Doppler signatures of the two modes are widely separated in the spectral domain, making the Doppler signatures corresponding to the two modes easy to separate. On the other hand, when f_δ is much smaller compared to Δf_{o} (i.e., $f_\delta \ll \Delta f_{\mathrm{o}}$), the O- and X-mode Doppler components are unresolvable in the spectral domain, resulting in a beating effect [30]. In this paper, we focus our consideration to the other case where the Doppler frequency profiles of the two propagation modes are resolvable but are close to each other or interlaced in the spectral domain. Such situations usually arise when $f_\delta \le 3\Delta f_{\mathrm{o}}$. In this case, the Doppler difference between the closest components in the two modes is smaller than Δf_{o}.

3 Doppler Signature Separation

In this section, we investigate the Doppler frequency separation by employing sparse signal processing. For this purpose, we exploit the Lasso algorithm [32] and, subsequently, reduce its complexity by employing a frequency focusing transform.

3.1 Sparsity-based Doppler Signature Separation

From [30], we know that all six Doppler components have the same chirp rate. Therefore, we can estimate the chirp-rate γ by employing a chirp transform [34] or fractional Fourier transform [35, 36]. Denoting $\hat{\gamma}$ as the estimated chirp-rate, the de-chirped form of the received OTHR signal is given as:

$$\begin{aligned} \bar{y}(t) &= y(t) e^{-j2\pi\hat{\gamma}t^2/2} \\ &\approx \sum_{i=1}^{3} \left(A_{\mathrm{o},i} e^{j(2\pi f^{\mathrm{s}}_{\mathrm{o},i} t + \phi_{\mathrm{o},i})} + A_{\mathrm{x},i} e^{j\left(2\pi f^{\mathrm{s}}_{\mathrm{x},i} t + \phi_{\mathrm{x},i}\right)} \right), \end{aligned} \tag{8}$$

where $f^{\mathrm{s}}_{\mathrm{o},i}$ and $f^{\mathrm{s}}_{\mathrm{x},i}$ denote the start frequencies respectively for the two modes after de-chirping.

In order to estimate the Doppler frequencies, we construct an $N \times 1$ data vector $\bar{\mathbf{y}}$ as:

$$\bar{\mathbf{y}} = [\bar{y}(t), \bar{y}(t-1), \cdots, \bar{y}(t-N)]^{\mathrm{T}}. \tag{9}$$

The sparse frequency estimation over the fine grid $\mathcal{F}$ consisting of R frequencies can be achieved using the Lasso algorithm as [32]:

$$\hat{\mathbf{r}} = \arg \min_{\mathbf{r}} ||\bar{\mathbf{y}} - \mathbf{F}\mathbf{r}||_2^2 + \zeta||\mathbf{r}||_1, \tag{10}$$

where $\mathbf{F}$ is the $N \times R$ inverse Fourier transform dictionary matrix with each of its columns corresponding to a frequency in $\mathcal{F}$, $\mathbf{r}$ is the $R \times 1$ sparse column vector, and $\zeta > 0$ is a regularization parameter. The positions of the non-zero elements of the obtained solution $\hat{\mathbf{r}}$ correspond to the estimated Doppler frequencies in the search grid, which are present in the de-chirped signal vector $\bar{\mathbf{y}}$.

3.2 Low-Complexity Implementation via Frequency Focusing

Recognizing that the Doppler frequencies occupy only a narrow spectrum bandwidth, we can reduce this computational complexity by decomposing the Lasso optimization (10) and enabling subband processing. This is realized by employing multiple frequency focusing transforms which enable concurrent processing of the received data on different processing chains dedicated for distinct subbands. The proposed strategy can also be exploited if the frequency band of interest is known a priori through, for example, coarse chirp parameter estimation in the previous stage. The proposed strategy not only reduces the search space of Lasso but also reduces the size of data vector $\bar{\mathbf{y}}$, resulting in a superior computational efficiency.

Let us construct a $B \times N$ frequency focusing matrix $\mathbf{B}$ (with $B \ll N$) whose B rows collectively cover a distinct subband of interest. The b-th row of $\mathbf{B}$ is given by:

$$[\mathbf{B}]_b = \frac{1}{N} \left[e^{j\left(\frac{N-1}{2}\right)b\frac{2\pi}{N}}, e^{j\left(\frac{N-3}{2}\right)b\frac{2\pi}{N}}, \cdots, e^{-j\left(\frac{N-1}{2}\right)b\frac{2\pi}{N}} \right], \tag{11}$$

which corresponds to a frequency sector centered at bf_s/N. The function of frequency focusing matrix $\mathbf{B}$ is analogous to the beamspace processing matrix [38] used in beamspace direction-of-arrival estimation problems which enables the data processing to be carried out only for a specific spatial sector of interest, thus significantly reducing the computational complexity.

The frequency focused data vector and the corresponding dictionary matrix take the following form:

$$\tilde{\mathbf{y}} = \mathbf{B}\bar{\mathbf{y}}, \quad \tilde{\mathbf{F}} = \mathbf{B}\mathbf{F}. \tag{12}$$

The new data vector $\tilde{\mathbf{y}}$ and the dictionary matrix $\tilde{\mathbf{F}}$ have dimensions $B \times 1$ and $B \times R$, respectively. Note the dimensions of $\tilde{\mathbf{y}}$ and $\tilde{\mathbf{F}}$ are much smaller than $\bar{\mathbf{y}}$ and $\mathbf{F}$, respectively.

The resulting optimization for frequency estimation using the frequency focused Lasso algorithm becomes

$$\begin{aligned} \hat{\mathbf{r}} &= \arg\min_{\mathbf{r}} ||\tilde{\mathbf{y}} - \tilde{\mathbf{F}}\mathbf{r}||_2^2 + \zeta||\mathbf{r}||_1 \\ &= \arg\min_{\mathbf{r}} ||\mathbf{B}(\bar{\mathbf{y}} - \mathbf{F}\mathbf{r})||_2^2 + \zeta||\mathbf{r}||_1. \end{aligned} \tag{13}$$

The computational complexity of Lasso exploiting the least angle regression (LARS) algorithm [37] for an $N \times 1$ data vector $\bar{\mathbf{y}}$ and an $R \times 1$ sparse vector $\mathbf{r}$ is given by $\mathcal{O}(R^3 + NR^2)$. In comparison, the corresponding computational complexity of the frequency focused Lasso is reduced to $\mathcal{O}(R^3 + BR^2)$. Considering that $NR \gg R^3 \gg BR^2$ typically holds, the frequency focused scheme provides significant improvement of the computational efficiency.

4 Simulation Results

In this section, we present simulation results that resolve the Doppler frequency components generated from the mixed O/X-mode signals. The key parameters are listed in Table I. We compare the performance between Lasso [32] and the proposed frequency focused Lasso approach. The search space for both algorithms is considered to be from 40 Hz to 42 Hz with a grid resolution of 0.005 Hz, resulting in $R = 400$ rows for the sparse vector $\mathbf{r}$. We use $B = 80$ rows $[\mathbf{B}]_b$, which correspond to uniformly spaced spectrum entries, in matrix $\mathbf{B}$ used to focus at the desired 2 Hz subband of interest. The simulations are performed on a computer equipped with Intel(R) Core(TM) i7-9750H (2.60 GHz) processor with 16 GB RAM. We used MATLAB R2021a (64-bit) and CVX toolbox (version 2.2, build 1148) [39].

Table 1 Simulation Parameters

Parameter	Notation	Value
Initial range	$R(0)$	2,500 km
O-mode ionosphere height	H	350 km
X-mode ionosphere height	$H - \Delta H$	335 km or 320 km
Target altitude	h	20 km
Target horizontal velocity	$\dot{R}$	400 m/s
Carrier frequency	f_c	16 MHz
Pulse repetition frequency	f_s	100 Hz
Coherent integration time	T	80 s
Signal-to-noise ratio (SNR)	η	0 dB

Two cases are considered below. In the first case, ΔH takes a small value, rendering interlaced multipath Doppler signatures. The second case considers an increased value of ΔH.

Case I ($\Delta H = 15$ km): The Doppler frequency profile for the mixed O/X-mode signals after de-chirping is illustrated in Fig. 4(a). It is observed that the six Doppler components are interlaced. For this case, the frequency estimation results using Lasso and proposed focused Lasso approaches along with their computational time are given in Figs. 4(b) and 4(c), respectively. It is evident that both algorithms are able to resolve all the Doppler signatures successfully. However, Lasso required more than 100 times of the computational time compared to the proposed frequency focused Lasso scheme.

Due to the fact that Doppler frequency components resulting from an individual propagation mode are equally spaced, the three components corresponding to each mode can be easily separated by inspecting the resolved Doppler signatures in this case.

Case II ($\Delta H = 30$ km): In this simulation, we consider a challenging case where all the six components resulting from the mixed O/X-mode signals are equally spaced. For this case, the actual Doppler signatures due to the mixed O/X-mode signals are illustrated in Fig. 5(a) whereas the frequency resolution results using Lasso and the proposed focused Lasso approach are presented in Figs. 5(b) and 5(c), respectively, along with their respective computation times. It can be noted that both algorithms provide similar frequency estimation results. However, the proposed frequency focused Lasso provides the estimation results in 0.78 sec compared to the conventional Lasso algorithm which requires 96.16 sec.

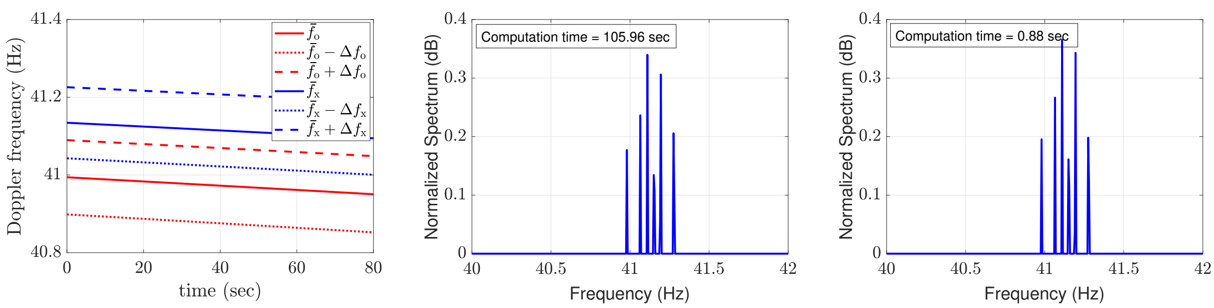

Actual Doppler signatures | Lasso [30] | Frequency focused Lasso (proposed)

Fig. 4. Doppler frequency estimation for interlaced Doppler signatures ($\Delta H = 15$ km, $N = 8,000$, $R = 400$, $B = 80$).

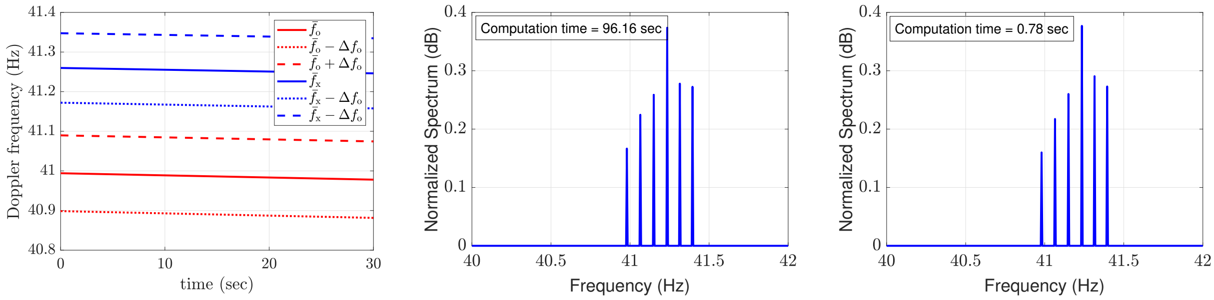

Actual Doppler signatures | Lasso [30] | Frequency focused Lasso (proposed)

Fig. 5. Doppler frequency estimation for proximal Doppler signatures ($\Delta H = 30$ km, $N = 8,000$, $R = 400$, $B = 80$).

For this specific case, because all components are equally spaced, there are two possible combinations of Doppler frequencies of O/X-mode signals which can generate such a result, namely, interleaved and side by side cases. In this case, additional information of the target and propagation status can be exploited from previous operations to identify the Doppler components corresponding to the two propagation modes.

5 Conclusion

In this paper, we investigated the Doppler frequency analysis for mixed O/X-mode OTHR signals when the virtual ionospheric heights for both modes exhibit a moderate height difference. It was observed that the frequency separation is challenging when the target Doppler frequencies of the two modes are interlaced or closely separated. In order to improve the efficiently in processing the Doppler signatures, a novel sparsity-aware frequency estimation strategy is proposed which exploits a frequency focusing transform to significantly reduce the computational complexity. Simulation results verified the effectiveness of the proposed strategy.

6 Acknowledgements

The work of A. Ahmed and Y. D. Zhang was supported in part by a contract with Matrix Research, Inc. for research sponsored by the Air Force Research Laboratory under Contract FA8650-14-D-1722. The work of Y. D. Zhang was also supported in part by a contract with Altamira Technologies Corp. for research sponsored by the Air Force Research Laboratory under Contract FA8650-18-C-1055.

7 References

[1] M. Headrick and M. I. Skolnik, "Over-the-horizon radar in the HF band," *Proc. IEEE*, vol. 62, no. 6, pp. 664–673, June 1974.

[2] Y. Zhang, G. J. Frazer, and M. G. Amin, "Concurrent operation of two over-the-horizon radars," *IEEE J. Sel. Top. Signal Process.*, vol. 1, no. 1, pp. 114–123, June 2007.

[3] J. M. Headrick and S. J. Anderson, "HF over-the-horizon radar," Chapter 20 in M. Skolnik (ed.), *Radar Handbook, 3rd Ed.* McGraw-Hill, 2008.

[4] G. A. Fabrizio, *High Frequency Over-the-Horizon Radar: Fundamental Principles, Signal Processing, and Practical Applications*. McGraw-Hill, 2013.

[5] G. J. Frazer, "Experimental results for MIMO methods applied in over-the-horizon radar," *IEEE Aerosp. Electron. Syst. Mag.*, vol. 32, no. 12, pp. 52–69, Dec. 2017.

[6] M. Papazoglou and J. L. Krolik, "Matched-field estimation of aircraft altitude from multiple over-the-horizon radar revisits," *IEEE Trans. Signal Process.*, vol. 47, no. 4, pp. 966–976, April 1999.

[7] R. H. Anderson, S. Kraut, and J. L. Krolik, "Robust altitude estimation for over-the-horizon radar using a state-space multipath fading model," *IEEE Trans. Aerosp. Electron. Syst.*, vol. 39, no. 1, pp. 192–201, Mar. 2003.

[8] D. Bourgeois, C. Morisseau, and M. Flecheux, "Over-the-horizon radar target tracking using multi-quasi-parabolic ionospheric modelling," *IEE Proc.-Radar, Sonar and Navig.*, vol. 153, no. 5, pp. 409–416, Oct. 2006.

[9] G. A. Fabrizio, G. J. Frazer and M. D. Turley, "STAP for clutter and interference cancellation in a HF radar system," *Proc. Int. Conf. Acoust. Speech, Signal Proc. (ICASSP)*, Toulouse, France, May 2006.

[10] H. Lan, Y. Liang, Q. Pan, F. Yang, and C. Guan, "An EM algorithm for multipath state estimation in OTHR target tracking," *IEEE Trans. Signal Process.*, vol. 62, no. 11, pp. 2814-2826, June 2014.

[11] J. Hu, M. Li, Q. He, Z. He, and R. S. Blum, "Joint estimation of MIMO-OTH radar measurements and ionospheric parameters," *IEEE Trans. Aerosp. Electron. Syst.*, vol. 53, no. 6, pp. 2789–2805,

[12] S. J. Anderson, "Target altitude estimation in OTHR via diffuse surface scatter," *Proc. IET Int. Radar Conf.*, Hangzhou, China, April 2015, pp. 1–6.

[13] H. Geng, Y. Liang, F. Yang, L. Xu, and Q. Pan, "Joint estimation of target state and ionospheric height bias in over-the-horizon radar target tracking," *IET Radar, Sonar & Navig.*, vol. 10, no. 7, pp. 1153–1167, Aug. 2016.

[14] H. Lan, Y. Liang, Z. Wang, F. Yang, and Q. Pan, "Distributed ECM algorithm for OTHR multipath target tracking with unknown ionospheric heights," *IEEE J. Sel. Topics Signal Process.*, vol. 12, no. 1, pp. 61–75, Feb. 2018.

[15] Z. Luo, Z. He, X. Chen, and K. Lu, "Target location and height estimation via multipath signal and 2D array for sky-wave over-the-horizon radar," *IEEE Trans. Aerosp. Electron. Syst.*, vol. 52, no. 2, pp. 617–631, April 2016.

[16] Y. D. Zhang, M. G. Amin, and G. J. Frazer, "High-resolution time-frequency distributions for manoeuvring target detection in over-the-horizon radars," *IEE Proc.-Radar Sonar Navig.*, vol. 150, no. 4, pp. 299–304, Aug. 2003.

[17] C. Ioana, Y. D. Zhang, M. G. Amin, F. Ahmad, G. Frazer, and B. Himed, "Time-frequency characterization of micro-multipath signals in over-the-horizon radar," *Proc. IEEE Radar Conf.*, Atlanta, GA, May 2012, pp. 671–675.

[18] Y. D. Zhang, M. G. Amin, and B. Himed, "Altitude estimation of maneuvering targets in MIMO over-the-horizon radar," *Proc. IEEE Sensor Array and Multichannel Signal Process. Workshop*, Hoboken, NJ, June 2012, pp. 257–260.

[19] Y. D. Zhang, J. J. Zhang, M. G. Amin, and B. Himed, "Instantaneous altitude estimation of maneuvering targets in over-the-horizon radar exploiting multipath Doppler signatures," *EURASIP J. Adv. Signal Process.*, vol. 2013, no. 2013:100, pp. 1–13, May 2013.

[20] C. Hou, Y. Wang, and J. Chen, "Estimating target heights based on the earth curvature model and micromultipath effect in skywave OTH radar," *J. Applied Math.*, vol. 2014, article 424191, pp. 1–14, July 2014.

[21] J. Hu, X. He, W. Li, H. Ai, H. Li, and J. Xie, "Parameter estimation of maneuvering targets in OTHR based on sparse time-frequency representation," *J. Systems Eng. Electron.*, vol. 27, no. 3, pp. 574–580, June 2016.

[22] Y. D. Zhang and B. Himed, "Multipath Doppler difference estimation in over-the-horizon radar," *Proc. IEEE Radar Conf.*, Oklahoma City, OK, April 2018.

[23] V. S. Amin, Y. D. Zhang, and B. Himed, "Modified Viterbi-based local-multipath Doppler difference estimation in over-the-horizon radar," *Proc. Asilomar Conf. Signals, Systems, and Computers*, Pacific Grove, CA, Oct. 2021.

[24] Y. D. Zhang, A. Ahmed, and B. Himed, "Target altitude estimation in over-the-horizon radar," *IEEE Access*, vol. 10, pp. 11260–11273, Jan. 2022.

[25] A. Ahmed, Y. D. Zhang, and B. Himed, "Joint target and ionosphere parameter estimation in over-the-horizon radar," *IEEE Trans. Aerosp. Electron. Syst.*, in press (doi: 10.1109/TAES.2022.3161396).

[26] A. Ahmed, Y. D. Zhang and B. Himed, "Doppler signature analysis of over-the-horizon radar signals with target altitude perturbation," *Proc. IEEE Radar Conf.*, New York, NY, Mar. 2022.

[27] J. M. Kelso, *Radio Ray Propagation in the Ionosphere*. McGraw-Hill, 1964.

[28] K. G. Budden, *The Propagation of Radio Waves: The Theory and Radio Waves of Low Power in the Ionosphere and Magnetosphere*. Cambridge University Press, 1985.

[29] T. J. Harris, M. A. Cervera, L. H. Pederick, and A. D. Quinn, "Separation of O/X polarization modes on oblique ionospheric soundings," *Radio Sci.*, vol. 52, pp. 1522–1533, Oct. 2017.

[30] A. Ahmed, Y. D. Zhang, and B. Himed, "Doppler signature analysis of mixed O/X-mode signals in over-the-horizon radar," *Proc. IEEE Int. Radar Conf.*, Rockville, MD, May 2020.

[31] A. Ahmed, Y. D. Zhang, and B. Himed, "Doppler signature separation of mixed O/X-mode over-the-horizon radar signals," *Proc. IEEE Radar Conf.*, Florence, Italy, Sept. 2020.

[32] R. Tibshirani, "Regression shrinkage and selection via the lasso," *J. R. Stat. Soc. B*, vol. 58, no. 1, pp. 267–288, 1996.

[33] N. Simon and R. Tibshirani, "Standardization and the group lasso penalty," *Stat. Sin.*, vol. 22, no. 3, pp. 983–1001, June 2012.

[34] L. R. Rabiner, R. W. Schafer and C. M. Rader, "The chirp z-transform algorithm and its application," *Bell Syst. Tech. J.*, vol. 48, no. 5, pp. 1249–1292, May-June 1969.

[35] E. Sejdić, I. Djurović, and L. Stanković, "Fractional Fourier transform as a signal processing tool: An overview of recent developments," *Signal Process.*, vol. 91, no. 6, pp. 1351–1369, June 2011.

[36] H. M. Ozaktas, M. A. Kutay, and Z. Zalevsky, *The Fractional Fourier Transform: With Applications in Optics and Signal Processing*. Wiley, 2001.

[37] B. Efron, T. Hastie, I. Johnstone, and R. Tibshirani, "Least angle regression," *Ann. Statist.*, vol. 32, no. 2, pp. 407–499, June 2004.

[38] H. L. Van Trees, *Optimum Array Processing: Part IV of Detection, Estimation, and Modulation Theory*. Wiley, 2001.

[39] M. Grant and S. Boyd, "CVX: Matlab software for disciplined convex programming," version 2.2, Build 1148, Jan. 2020. http://cvxr.com/cvx.